# The extended law of corresponding states when attractions meet repulsions

van Gruijthuijsen, K.; Obiols-Rabasa, M.; Schurtenberger, P.; Bouwman, Wim; Stradner, A.

**Important note**
To cite this publication, please use the final published version (if applicable).
Please check the document version above.

# Soft Matter

ROYAL SOCIETY
OF CHEMISTRY

# The extended law of corresponding states when attractions meet repulsions

K. van Gruijthuijsen, †*[a] M. Obiols-Rabasa, ‡[b] P. Schurtenberger, [b] W. G. Bouwman [c] and A. Stradner [b]

Short-range attractive colloids show well-defined phase behaviour in the absence of repulsions, and highly intriguing equilibrium gelation in the presence of long-range repulsions. We present the state diagram of short-range attractive colloids with repulsions that range from fully screened to intermediately ranged, *i.e.* longer-ranged than the attractions, but shorter ranged than the colloid size. We demonstrate that although the macroscopic phase behaviour does not change perceptibly, there is a dramatic increase of inhomogeneities once the repulsions become longer-ranged than the attractions. The interaction potentials are characterized with small angle neutron scattering, and used to renormalize the state diagram with the minimum in the interaction potential, min[$U(r)$], and with the reduced second virial coefficient, $B_2^*$. We find that the extended law of corresponding states captures the onset of phase separation for shorter ranged repulsions, but fails for longer ranged repulsions. Instead, for a given model of $U(r)$, the transition from visually homogeneous fluid to phase separation and/or gelation can be rescaled with min[$U(r)$] over the full range of repulsions. Finally, we suggest a generic state diagram to describe the effect of repulsions on short-range attractive systems.

## 1 Introduction

Colloidal gels are widely applied in food products and other materials.[1,2] The required attractive colloid–colloid potential can be induced by the passive use of van der Waals (vdW) or hydrophobic interactions, or actively controlled by a polymer-induced depletion potential. It is now generally accepted, that as long as the attractions are short-ranged, *i.e.* the interaction range $\gamma$ is less than about 10% of the colloid diameter $2R$, the associated equilibrium phase behaviour is universal: if sufficiently monodisperse and given enough time, the colloids undergo crystallization, which can be preceded at shorter times by a meta-stable fluid–fluid coexistence. In contrast, no consensus exists on the non-equilibrium phase behaviour of short-range attractive systems, notably on the position of the gel and glass lines.[3–5] Comparison between typical model systems such as poly(methyl methacrylate) (PMMA) particles and globular proteins is hampered by the additional presence and proper characterization of screened Coulomb repulsions and by density mismatching,[6] as well as by a certain degree of anisotropy in the

interaction potential of proteins that may arise from patches frequently occurring on the protein surface.[7,8] In this paper, we further address this issue and we map the phase behaviour of well-defined aqueous model colloids that interact *via* polymer-induced short-range attractions and variably-ranged repulsions.

Following the extended law of corresponding states (ELCS), the state diagram of short-range attractive colloids with residual repulsions can be renormalized using a reduced second virial coefficient, $B_2^* = 3B_2/16\pi R^3$, as an effective temperature, with $B_2$ the second virial coefficient and $R$ the colloid radius, and $B_2^*$ given by:[9]

$$B_2^* = \frac{1}{m} + \frac{3}{8mR^3}\int_{2R}^{\infty}[1 - \exp(-\beta U(r))r^2 \mathrm{d}r] \tag{1}$$

with

$$m^{1/3} = 1 + \frac{1}{2R}\int_{2R}^{\infty}[1 - \exp(-\beta U_{ES}(r))]\mathrm{d}r \tag{2}$$

here $U(r)$ is the overall interaction potential between two colloids with a center-to-center distance of $r$, while $U_{ES}(r)$ represents the electrostatic contribution to the interaction potential. For a given temperature $T$, $\beta = (k_B T)^{-1}$ becomes a constant, with $k_B$ the Boltzmann constant. The parameter $m^{1/3} = R_{eff}/R$ defines an effective hard sphere interaction radius for colloids with screened coulomb repulsions,[10–12] and is thus an indicator for the range of the repulsions. These concepts were successfully applied to describe equilibrium crystallization of protein solutions,[13–15]

[a] *Adolphe Merkle Institute, University of Fribourg, Chemin des Verdiers 4, CH-1700 Fribourg, Switzerland. E-mail: Kitty.vanGruijthuijsen@gmail.com*

[b] *Division of Physical Chemistry, Department of Chemistry, Lund University, Naturvetarvägen 16, SE-223 62 Lund, Sweden*

[c] *Delft University of Technology, Mekelweg 15, 2629 JB Delft, The Netherlands*

† Present address: Firmenich SA, Meyrin, Switzerland.

‡ Present address: CR Competence AB, Lund, Sweden.

and meta-stable fluid–fluid phase separation in proteins and polymeric colloids.[3,5] It has been suggested that $B_2$*-scaling can be applied to non-equilibrium gelation and the glass transition as well.[3,4] In contrast, it was found for lysozyme that the location of the glass transition was determined by the value of the contact potential, $U(2R)$, rather than by $B_2$*, which is an integral measure of the interaction potential.[5]

Due to their small size, proteins tend to exhibit relatively longer ranged repulsions. For intermediate repulsive ranges, *i.e.* repulsions are longer-ranged than the attractions, but shorter-ranged than the protein size, $B_2$-scaling accurately captures crystallization as well as fluid–fluid phase separation.[5,14] Once the repulsions become longer-ranged than the protein diameter, they can stabilize growing clusters.[16] Such equilibrium clusters have been observed in proteins in aqueous solutions,[16–18] and in colloid dispersions in organic solvents.[18–21] Gelation in the presence of repulsions that are longer-ranged than the colloid size becomes an equilibrium process,[17,19–23] with immense industrial potential. However, thus far, the cross-over between these regimes is poorly understood.

The study of intermediate-ranged repulsions in polymeric colloids is often hampered by strong vdW attractions in aqueous systems,[24] and limited tuneability of the repulsions in organic solvents.[25] Here, we present the state diagram of sterically stabilized, charged polystyrene colloids in water mixed with poly(ethylene oxide) (PEO) polymer chains. We use colloids with a well-defined colloid volume fraction, $\phi$, and effective surface charge, $Z_{eff}$, as characterized with small angle neutron and X-ray scattering (SANS and SAXS) and spin-echo SANS (SESANS).[26,27] Varying the concentration of monovalent salt (NaCl and/or NaN$_3$), $c_s$, between 100 mM and 1.5 mM we access fully screened to intermediate-ranged repulsions. Water is a good solvent for PEO, and the polymer size is chosen such that the depletion-induced attractions are short-ranged compared to the colloid radius. The range of the attractive potential is given by $\gamma = R_g/R$, with $R_g$ the radius of gyration of the polymer, and the depth is controlled by the polymer concentration.[28]

## 2 Materials and methods

### 2.1 Materials

Three different batches of polystyrene colloids (MA2, MA3 and MA4) are synthesized, purified and characterized as described previously.[26,27] The colloids are negatively charged by copolymerisation with methacrylic acid, and sterically stabilized by chemically grafted Tween 80, which forms a dense shell with $\sim$2 nm alkyl chains bound to the polystyrene and $\sim$2 nm PEO chains protruding into the solution.[26] To adjust the contrast for the various scattering techniques, colloids MA2 and MA3 are prepared in H$_2$O and colloids MA4 in D$_2$O. The properties of the colloids and their stock solutions are summarized in Table 1. The polydispersity of colloids MA2 and MA3 was found to be around 8% and is assumed to be comparable for colloids MA4.[26]

Poly(ethylene oxide) (PEO) polymer is purchased from Polymer Source and used without further purification. Its number and weight averaged molecular weights, as given by the supplier, are respectively $M_n$ = 12.3 kg mol$^{-1}$ and $M_w$ = 13.3 kg mol$^{-1}$. Based on literature data for PEO, we calculate the radius of gyration to be $R_g$ = 0.99$M_w^{0.60}$ = 4.7 nm,[29–34] and the overlap concentration $c^* = 3M_w/4\pi N_A R_g^3$ = 51 g L$^{-1}$ with $N_A$ being Avogadro's number.[29]

### 2.2 Phase diagram

Colloid/polymer mixtures are prepared by mixing appropriate amounts of stock solutions of the colloids and the polymer (with $c_s$ = 0 or 3 mM), and additional quantities of deionised water and/or more concentrated salt solutions. For mixtures with colloids MA2 we use H$_2$O, for colloids MA3 a mixture of H$_2$O/D$_2$O at 84/16 volume fractions, and for colloids MA4 we use D$_2$O as the solvent. Low salt solutions ($<$5 mM) are all prepared with sodium azide to prevent microbial growth, while sodium chloride is used to obtain solutions $>$5 mM.

Colloids MA2 are used to establish the full state diagram. The samples are weighted in an Eppendorf tube and homogenized by vortexing during 30 s (MS1 Minishaker, IKA). About 0.2 mL is pipetted into a rectangular glass cell with dimensions 1 $\times$ 10 mm$^2$ (Yixing Zhicheng Material) that is closed with epoxy glue to prevent evaporation. Thus, sample heights are about 20 mm. For the SANS measurements, mixtures with colloids MA3 are prepared in a solvent containing 16 vol% D$_2$O, to minimize multiple scattering of neutrons and to match the PEO scattering.[26] The SESANS measurements are performed with colloids MA4 in D$_2$O to maximize the scattering.[27]

Transmission height profiles are measured with the Profiler (in-house design with components all from Thorlabs, see ref. 12). A laser beam with wavelength $\lambda$ = 633 nm is guided through a sample holder, which can contain up to five square cells, to a standard power sensor (400–1100 nm, 50 mW) with a laser line filter (632.8 nm). Two high precision motors control the horizontal motion between sample positions, and the vertical scan through the samples to obtain the transmission height profile (THP).

**Table 1** Characteristics of the used colloids and their concentrated stock solutions

| Batch | $c^a$ [g L$^{-1}$] | $c_s{}^b$ [mM] | $R^c$ [nm] | $c/\phi^c$ [kg L$^{-1}$] | $Z_{eff}{}^c$ | Method$^c$ | $\gamma$ |
|---|---|---|---|---|---|---|---|
| MA2 | 406 | 3.0 | 55.5 ± 1 | 0.955 | 500 ± 50 | SAXS[26] | 0.085 |
| MA3 | 452 | 2.0 | 62 ± 2 | 1.040 | 550 ± 50 | SANS, SAXS[26] | 0.076 |
| MA4 | 352 | 2.0 | 61 ± 1 | 1.060 | 550 ± 50 | SESANS, SAXS[27] | 0.077 |

$^a$ Concentration of stock solution, measured with a Moisture Analyzer MA35 (Sartorius). $^b$ Sodium azide concentration in stock solution. $^c$ Hard sphere radius $R$, volume fraction $\phi$, and effective surface charge $Z_{eff}$ for $c_s$ = 50 mM, determined from SANS, SAXS and SESANS according to ref. 26 and 27 and using $U_{ES,SC}(r)$ in eqn (4).

## 2.3 Scattering techniques

Mixtures with colloids MA3 are characterized with small angle neutron scattering (SANS) at the SANSI instrument at the Paul Scherrer Institute in Villigen, Switzerland.[35] We use neutrons with $\lambda$ = 1.2 nm (10% wavelength spread), which are collimated over 18 m, focused on the sample by 11 neutron lenses, and scattered neutrons are collected at a sample-detector distance of 20 m. Samples are measured in 1 mm quartz cells (120-QS, Hellma). Scattering intensities are corrected for detector efficiency and scaled to absolute scattering cross-sections, $d\Sigma/d\Omega$, using a water measurement at 4.5 m sample-detector distance and 4.5 m collimation.[36] The covered $q$-range is 0.009–0.2 nm$^{-1}$, where the scattering vector $q = 4\pi \sin(\theta/2)/\lambda$ with $\theta$ the scattering angle. Structure factors $S(q)$ are computed by dividing the concentration-normalized scattering intensities by the concentration-normalized intensity of a dilute sample with $c$ = 10 g L$^{-1}$, which is considered to be interaction free.

Mixtures with colloids MA4 are measured with SESANS at the Reactor Institute Delft (Delft, the Netherlands).[37] SESANS measures the polarization of a neutron beam, here with $\lambda$ = 0.21 nm and a cross-section defined by a pinhole of 16 × 10 mm$^2$, which passes through two vertical effectively parallelogram-shaped magnetic fields with opposite field directions, and inclination angle $\theta_0$. Polarized neutrons travelling through these fields perform a precession with exactly opposite precession angles in the first and the second field. Scattering by a sample, placed between the two fields, is detected as a depolarisation compared to that of the empty beam, $P_m(z)$. The spin-echo length, $z = C\lambda^2 Bl_{MF} \cot[\theta_0/2\pi]$, is varied by the variation of the magnetic-field strength, $B$. The constant $C$ equals $4.6368 \times 10^{14}$ T$^{-1}$ m$^{-2}$, $L$ = 4 mm is the path length through the sample, and $l_{MF}$ is the travel distance of the neutrons through the magnetic fields.[38]

Colloids MA2, MA3 and MA4 have been characterized by small angle neutron scattering (SANS) as well, as described previously.[26,27] Unfortunately, the presence of larger amounts of PEO required for the lower salt concentrations, strongly influences the X-ray contrast profile of the core–shell colloids, hampering the use of SAXS to characterize mixed potentials for $c_s$ < 20 mM. Therefore, we only use the SANS and SESANS results for mixtures with colloids MA3 and MA4 to model interaction potentials. For colloids MA2, hypothetical potentials are deduced, that would align the observed phase behaviour with the apparent trends for colloids MA3 and MA4.

## 2.4 Two models for the interaction potential

SANS and SESANS data are modelled using two different approaches to describe the interaction potential $\beta U(r)$:

$$\beta U(r) = \begin{cases} \infty & \text{for } r < 2R \\ \beta U_{ES}(r) + \beta U_{dep}(r) & \text{for } r \geq 2R \end{cases} \quad (3)$$

The first approach combines screened Coulomb (SC) repulsions and the Asakura–Oosawa (AO) depletion potential, given by:[27]

$$\beta U_{ES,SC}(r) = \frac{Z_{eff}^2 l_B \exp(-\kappa(r-2R))}{r(1+\kappa R)^2} \quad (4)$$

with the inverse Debye screening length:

$$\kappa = \left( \frac{3l_B Z_{eff}\varphi}{(1-\varphi)R^3} + 8\pi l_B c_s N_A \right)^{0.5} \quad (5)$$

The depletion attractions follow:

$$\beta U_{dep}(r) = \begin{cases} \dfrac{-\Pi\left(\gamma' - \dfrac{r}{2R}\right)\left(\gamma' + \dfrac{r}{4R}\right)}{\gamma^3(1-\phi\gamma'^3)} & \text{for } 2R \leq r \leq 2R\gamma' \\ 0 & \text{for } r > 2R\gamma' \end{cases}$$

$$(6)$$

here $l_B \approx 0.7$ nm is the Bjerrum length in water, the polymer osmotic pressure $\Pi$ corresponds to $\Pi_{AO} = \phi_p = c_p/c^*$ for AO attractions, with $\phi_p$ the swollen polymer volume fraction expressed as the polymer concentration $c_p$ normalized by the overlap concentration $c^*$, and the range of the attractions is given by $\gamma_{AO}' = (\gamma + 1)$ with $\gamma = R_g/R$.

The second approach uses empirically adjusted analytical expressions that mimic accurate interaction potentials that were deduced from a full theoretical description of the system, combining classical polymer density functional (DF) theory for the polymer-mediated attractions and fully non-linear Poisson–Boltzmann (nlPB) theory for the electrostatic repulsions.[39] The strong short-range repulsions predicted by Poisson–Boltzmann (PB) theory are mimicked by a double Coulomb potential:

$$\beta U_{ES,PB}(r) = \beta U_{ES,SC}(r) + \frac{20Z_{eff}^2 l_B \exp(-3\kappa(r-2R))}{r(1+3\kappa R)^2} \quad (7)$$

The AO potential is a simplified expression that assumes ideal behaviour for the polymer, *i.e.* theta solvent conditions and concentrations significantly below the overlap concentration. In fact, water is a good solvent for PEO, and we use concentrations approaching the overlap concentration. Therefore, the AO potential is adjusted with analytical expressions for good solvent (GS) conditions for the range of the attractions:[40]

$$\gamma_{GS} = 0.865 \left[ \frac{\gamma}{\sqrt{1+3.95\phi_p^{1.54}}} \right]^{0.88} \quad (8)$$

as well as for the scaling of the osmotic pressure with the polymer concentration:[40]

$$\Pi_{GS} = 0.83[\phi_p + 3.77\phi_p^{2.31}] \quad (9)$$

The good-solvent potential $U_{dep,GS}$ is obtained by inserting $\gamma_{GS}' = (\gamma_{GS} + 1)$ and $\Pi_{GS}$ in eqn (6). The pre-factor 0.83 is empirically estimated to match the DF results,[39] and in line with a ~20% overestimation of the part in brackets in eqn (9).[40]

Fig. 1 shows a comparison of the various potentials for colloids MA3 in 50 and 1.5 mM salt and polymer concentrations close to the gel transition, using the same parameters as in ref. 39. Although there is still a quantitative discrepancy between the more accurate DF–nlPB potentials and the empirical GS–PB potentials, the GS–PB captures the qualitative properties
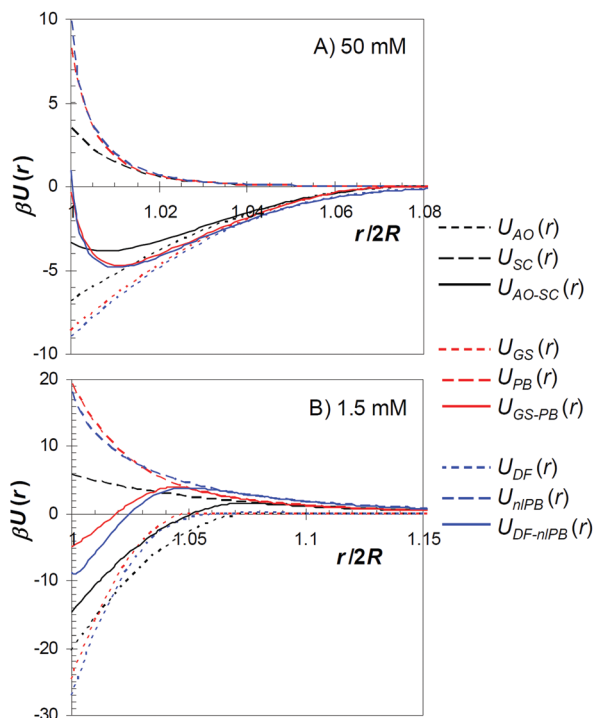
**Fig. 1** Interaction potentials for colloids MA3, based on the parameters used in ref. 39 ($\phi = 0.215$, $Z_{eff} = 275$ and $c_p = 37.6$ g L$^{-1}$ for $c_s = 1.5$ mM, and $Z_{eff} = 1100$ and $c_p = 12.7$ g L$^{-1}$ for $c_s = 50$ mM), and calculated using Asakura–Oosawa attractions and screened Coulomb repulsions (AO–SC), good solvent attractions and mimicked Poisson–Boltzmann repulsions (GS–PB), and density functional theory attractions and fully non-linear Poisson–Boltzmann repulsions (DF–nlPB; ref. 39).

of the DF–nlPB reasonably well. Notably, there is a profound difference with the more simplistic AO–SC potentials.

### 2.4 Modelling of scattering data

$U_{AO–SC}(r)$ and $U_{GS–PB}(r)$ are used to compute the structure factor $S(q)$ by numerically solving the Ornstein–Zernike equation with the Percus–Yevick closure relation.[41] For the rather low polydispersity of the colloids below 10%, the calculated monodisperse $S(q)$ forms a good approximation of the real polydisperse structure factor.[42]

From the SANS measurements of colloids MA3, experimental $S(q)$s are directly accessible. Previously, we established the constant $c/\phi$ and $Z_{eff,SC}(\phi,c_s)$ for a colloid/salt concentration series in the absence of polymer using SC repulsions.[26,27] Upon the addition of PEO, only the parameter $Z_{eff,SC}(\phi,c_s,c_p)$ is allowed to vary to optimise the agreement between the experimental and computed $S(q)$. In a comparable way, we establish $Z_{eff,PB}(\phi,c_s,c_p)$ using $U_{GS–PB}(r)$.

For the SESANS measurements of colloids MA4, the computed $S(q)$s are used to calculate the scattering intensity $I(q)$ using the theoretical form factor $P(q)$ for monodisperse, homogeneous hard spheres:[43]

$$I(q) = \frac{4}{3}\pi R^3 \phi (\Delta\rho)^2 P(q) S(q) \quad (10)$$

here $\Delta\rho$ is the excess scattering length density of the colloids in the continuous phase, which consists of D$_2$O and PEO. From $I(q)$ we can calculate $G(z)$, which is defined as the projection of the autocorrelation function of the scattering length density distribution along the direction of the SESANS neutron beam:[38]

$$G(z) = \int_0^\infty J_0(qz)I(q)q\mathrm{d}q \quad (11)$$

here $J_0$ is the zeroth-order Bessel function of the first kind. The measured neutron depolarisation $P_m(z)$ can be related to $G(z)$ according to:[38,44]

$$\ln[P_m(z)]/L = \lambda^2[G(z) - G(0)]/2\pi \quad (12)$$

The aim of the modelling procedure is to apply a consistent approach to link scattering data, interaction potentials, and reduced virial coefficients. Using both the AO–SC and GS–PB potential in this procedure allows a comparison of two significantly different model descriptions, while keeping the computational investment to a minimum. Determined $Z_{eff}$ values will be discussed in terms of qualitative trends, rather than absolute values. It should be kept in mind that the colloids are sterically stabilized, with the surface charges probably distributed within the $\sim 2$ nm PEO steric layer. We previously found a reduced grafting density $> 1$,[26] which supports the assumption that the colloids behave as hard spheres with respect to the free PEO chains. Nevertheless, some limited softness might affect the detailed phase behaviour.

## 3 Results and discussion

### 3.1 State diagram

To establish the state diagram of colloids interacting *via* short-range attractions and variably ranged repulsions, colloids MA2 with an effective hard sphere radius of $R = 55.5$ nm are mixed with poly(ethylene oxide) (PEO) polymer with a radius of gyration of $R_g = 4.7$ nm. The range of the attractive potential is defined as the size ratio $\gamma = R_g/R = 0.085$. The steric PEO shell on the colloids renders them hard spheres at high salt concentrations, and additionally prevents free PEO from adsorbing on the surface. The only drawbacks of such a system are the density mismatch and the high refractive index difference between polystyrene and water. Although it is possible to density match polystyrene colloids in an appropriate mixture of H$_2$O and D$_2$O, we decided to maintain a density difference to accelerate phase separation processes, and bear in mind that the phase behaviour might be affected by gravity. The latter drawback hinders visual observations of the samples due to multiple light scattering. This effect is reduced by preparation of the samples in flat rectangular cells with a thickness of 1 mm. Sharp interfaces can be observed by back-illumination with a LED flash light in a dark room. To further quantify the phase behaviour, we use our Profiler, where the transmitted laser light intensity is measured as a function of height in the sample at several moments after mixing,[12] and which we refer to as the transmission height profile (THP).
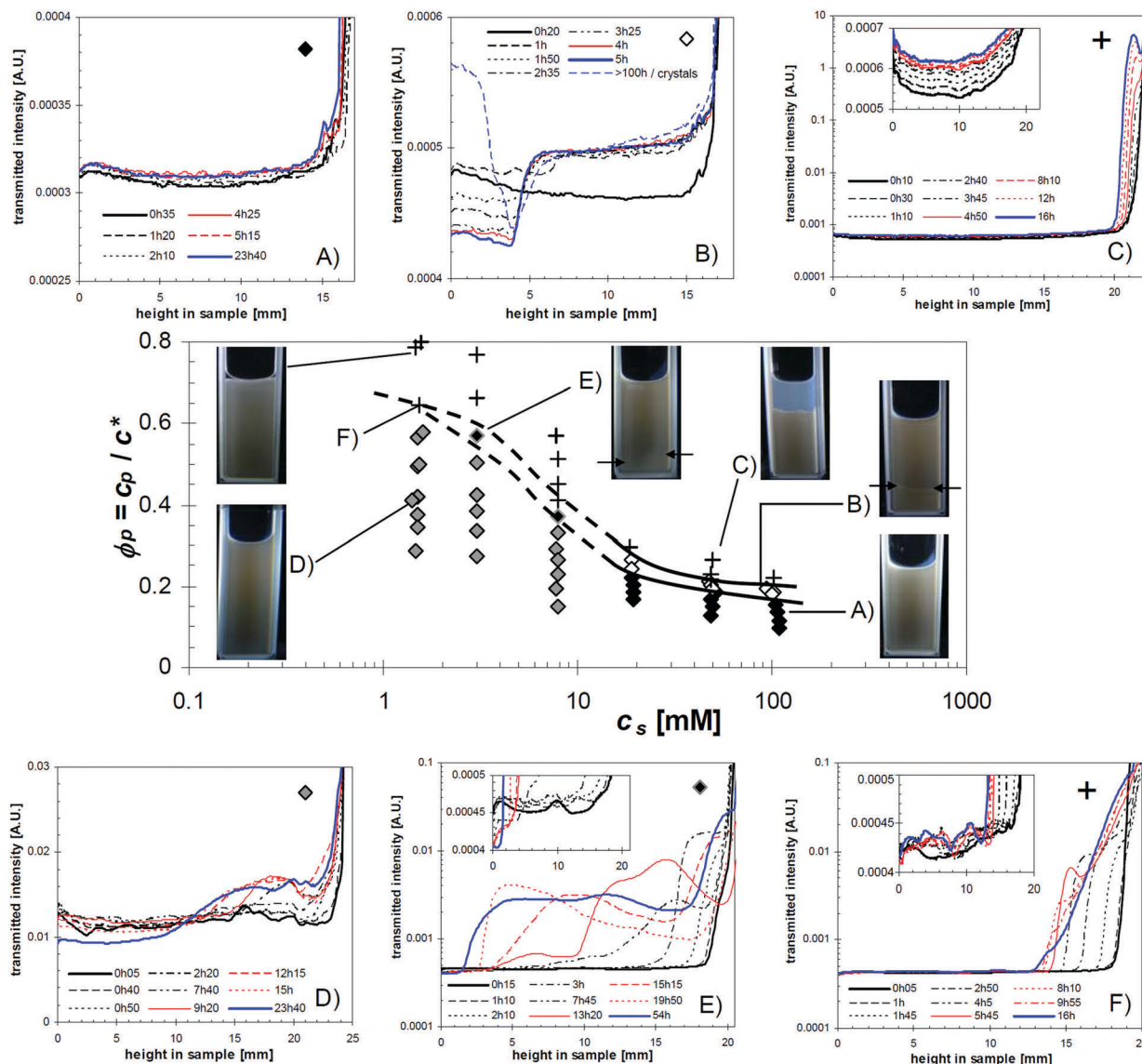
Fig. 2  State diagram of colloids MA2 and PEO polymer with a size ratio $\gamma = 0.085$ and colloid volume fraction $\phi = 0.20$. Phases are allocated based on visual appearance and transmission height profile (THP). Typical profiles for each type of phase behaviour are shown in graphs A to F. Symbols correspond to visually mixed samples with a flat THP (full diamonds, A), samples with a clear interface that forms at a specific height and stays there (open diamonds, B), gelled samples where a visible interface forms at the top, the position of which decreases with time (plus symbols, C and F), visually homogeneous samples that form a gradient in the THP (grey-black diamonds, D), and samples with a visible interface where the THP strongly fluctuates with time (black-grey diamonds, E). Lines in the state diagram are drawn to guide the eye. The legends in graphs (A–F) indicate the time after mixing; the $y$-axes are chosen to cover the variation in transmitted intensity in each sample. The steep upturn in the profile at the top of the samples reflects the meniscus at the air–water interface. The pictures in the main graph were taken several months after recording the THPs.

Interestingly, our – rather crude – methodology to study the colloid/polymer mixtures opens up a wealth of information, as summarized in Fig. 2. For the higher salt concentrations, 100 mM, 50 mM, and 20 mM, the behaviour typical for short-range attractive systems is retrieved. At low polymer concentrations the samples appear homogeneous and have a flat THP, *i.e.* they are truly in the mixed state and do not evolve over time.

At a well-defined polymer concentration, an interface appears that corresponds to a step in the THP, as exemplified in Fig. 2B. The position of this interface does not change significantly with time, but the flat THPs of the upper and lower phase increasingly deviate with time. This is typical for equilibrium fluid–fluid phase separation into a colloid-poor upper phase with a higher transmission and a colloid-rich lower phase with a lower transmission. Note that in these samples the lower phase will crystallize within several days, confirming that the polydispersity is below 15%. Due to the long-range order in the crystals, the transmission is higher than that of the liquid colloid-rich phase.

At a higher, well-defined polymer concentration the interface is formed at the top of the samples and moves down with time like in Fig. 2C and F. We consider these samples to be collapsing

gels, where the transmission of the upper phase is several orders of magnitude higher than that of the phase separating samples. Here the phase separation process leads to a space-spanning and gravitational stress-bearing network. After about 1 h 30 the gel network in Fig. 2C collapses under its own weight. Even after 8 months, the time at which the image of this sample is taken, there is no indication of crystallization, confirming the truly arrested state of the colloid-rich phase. As expected, with decreasing salt concentration, *i.e.* increasing repulsions, more polymer is required to induce the phase transitions, but phenomenologically the phase behaviour does not change.[10,45]

A further reduction of the salt concentration from 20 mM to 8 mM dramatically alters the phase behaviour of the colloid/polymer mixtures. Visually, the samples demonstrate the same behaviour: homogeneous at low polymer concentrations; the development of an interface at higher polymer concentrations; finally forming a gel. However, the THPs portray quite a different picture. In general, they show very strong vertical gradients and inhomogeneities that extend over several millimetres. Even the gels, *i.e.* those samples that have an interface that is gradually lowered, feature height dependent transmissions of the upper phase, as it appears in Fig. 2F.

In the state diagram, the lines indicating the sharp phase transitions at high salt are therefore only tentatively extended as dashed and dotted lines to low salt concentrations. Notably between the visually homogeneous samples and those with a visible interface, depicted in Fig. 2D and E, the inhomogeneities in the THPs gradually increase with increasing polymer concentration. At this point we can not conclude whether these samples undergo true phase transitions. However, the vertical gradients imply that gravity plays a role, which in turn suggests the formation of either larger clusters or aggregates of colloids[18,20] or at least a difference in average colloid concentration.

We expect that the range of the repulsions $\gamma_{ES}$ compared to that of the attractions ($\gamma = 0.085$) is the decisive parameter for the onset of inhomogeneities.[46] Table 2 lists $\gamma_{ES,SC}$ as a function of salt concentration expressed as either the reduced Debye length $(\kappa R)^{-1}$ or as the effective radius $m^{1/3}$.[26] A naïve assumption would be that the phase behaviour changes once the characteristic range of the repulsions $((\kappa R)^{-1}$ and/or $m^{1/3})$ becomes longer-ranged than the attractions ($\gamma = 0.085$), which would coincide with a change for $\leq 3$ mM. The observed onset of inhomogeneities already at $\leq 8$ mM indicates a more complex relation. To put these results into perspective, we will

first determine interaction potentials for the whole data set, and attempt to rescale the state diagram as discussed in the introduction. Finally, we will use these results to rationalize the observed inhomogeneities.

## 3.2 Rescaled state diagram with $U(r)$

Though phenomenologically clear, the state diagram in Fig. 2 expressed in absolute polymer and salt concentrations cannot be easily translated to other systems. As postulated in the introduction, the system under study is expected to follow the extended law of corresponding states (ELCS), which dictates that the state diagram of short-range attractive colloids can be rescaled by the reduced second virial coefficient $B_2*$.[9] At the same time, some studies indicate that the contact value of the interaction potential is the relevant parameter to rescale the non-equilibrium gel transitions of the state diagram.[5]

A large series of mixtures of colloids MA3 (SANS) or MA4 (SESANS) with PEO at various colloid, polymer and salt concentrations has been modelled using the AO–SC and GS–PB potentials. Fig. 3 shows the results for the most relevant samples with $\phi$ close to 0.2. The two different potentials yield basically identical descriptions of the experimental data, capturing well the development of the position of the first structure factor peak.

In contrast, the $Z_{eff}$ values required to obtain these results vary widely, as shown in Fig. 4A for the AO–SC potential and in Fig. 4B for the GS–PB potential. Charge renormalization is found to be a function of polymer as well as salt and colloid concentration for both potentials. Thus, the addition of short-range attractions to longer-ranged repulsions can reverse
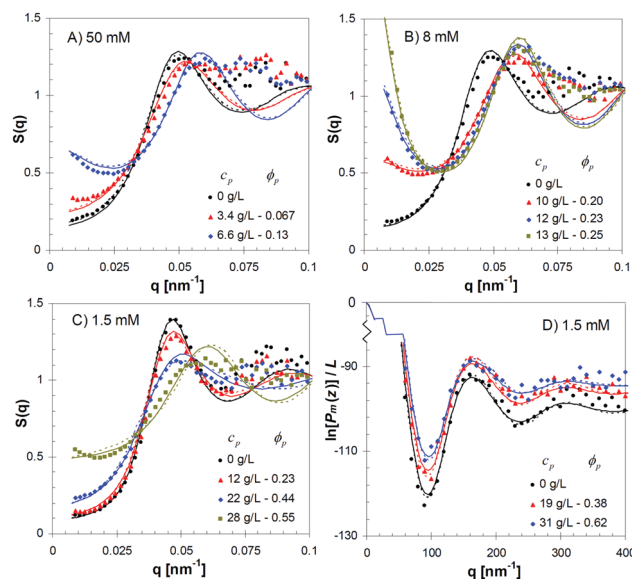


**Fig. 3** SANS structure factors of mixtures of colloids MA3 and PEO with $c_s$ = (A) 50 mM, (B) 8 mM and (C) 1.5 mM for = 0.22. (D) SESANS data of mixtures of colloids MA4 and PEO with $c_s$ = 1.5 mM for $\phi$ = 0.21. In all images, symbols depict experimental data, dotted lines indicate calculations using the AO–SC model, and continuous lines indicate calculations using the GS–PB model as described in the main text.

**Table 2** Range of the SC repulsive potential for colloids MA2

| $c_s$ [mM] | $Z_{eff}{}^a$ | $(\kappa R)^{-1}$ | $m^{1/3}$ |
|---|---|---|---|
| 100 | 500 | 0.017 | 1.004 |
| 50 | 500 | 0.025 | 1.010 |
| 20 | 500 | 0.039 | 1.028 |
| 8 | 430 | 0.061 | 1.059 |
| 8 | 500[b] | 0.061 | 1.068 |
| 3 | 370 | 0.099 | 1.12 |
| 1.5 | 180 | 0.14 | 1.11 |

[a] According to ref. 26 for $c_p = 0$ g L$^{-1}$ and with 10% uncertainty in $Z_{eff}$.
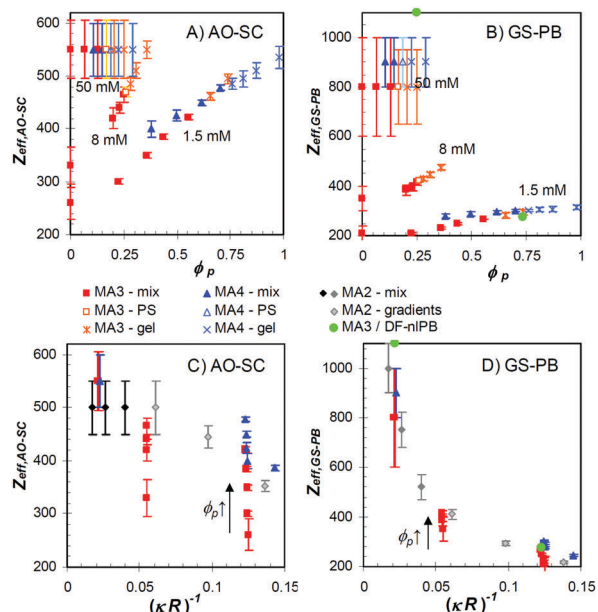[b] Hypothetical case, added for comparison.

**Fig. 4** Effective surface charges of colloids MA3 (red symbols: $\phi = 0.22$) and MA4 (blue symbols: $\phi = 0.21$) as a function of salt (data labels in A and B) and polymer concentration as determined by respectively SANS and SESANS for "mix" samples using (A and C) the AO–SC model, and (B and D) the GS–PB model; surface charges for phase separated (PS) and gelled samples are estimated by linear extrapolation (grey, orange and light blue symbols). Error bars are manually estimated and indicate the values between which a reasonable fit with the data is obtained. (C and D) Estimated effective surface charges of colloids MA2 ($\phi = 0.20$) close to the phase transitions from SAXS (black symbols) and hypothetically (grey symbols) as explained in the main text.

decreased surface charges under intermediate screening conditions. This is a rather surprising finding, as the SANS data of MA3 colloids with $c_s = 1.5$ mM were previously modelled with a combination of a highly accurate density functional theory description of the polymer-mediated attractions, and fully non-linear Poisson–Boltzmann repulsions with a fixed value of $Z = 275$.[39] It should be noted, though, that the agreement between modelled and experimental data in Fig. 3A and C is consistently closer than in ref. 39.

The state diagram for colloids MA3 and MA4 is plotted as a function of the contact potential, which we express here as the local minimum of $\beta U(r)$ at $2R < r < 1.02(2R)$, to account for the typical shape of $U_{GS-PB}(r)$ for higher salt concentrations (Fig. 1A). For the AO–SC potentials, $\min[\beta U_{AO-SC}(r)]$ is identical to the more rigid definition of the contact potential as $\beta U_{AO-SC}(2R)$. Fig. 5 shows that the first transition from visually homogeneous fluid samples to either phase separated ($c_s \geq 8$ mM) or gelled samples ($c_s = 1.5$ mM) can be fully rescaled with $\min[\beta U(r)]$, independent of the used model. Nevertheless, the absolute values of the phase transition vary slightly, with $\min[\beta U_{AO-SC}(r)] = -3.8 \pm 0.1$ and $\min[\beta U_{GS-PB}(r)] = -3.5 \pm 0.1$.

Since limited to no charge renormalization was observed for the SC potential in the absence of PEO polymer (Table 2), $Z_{eff,sc} = 500 \pm 50$ was used to calculate the state points for colloids MA2 and $c_s \geq 8$ mM. Fig. 5A shows that these data
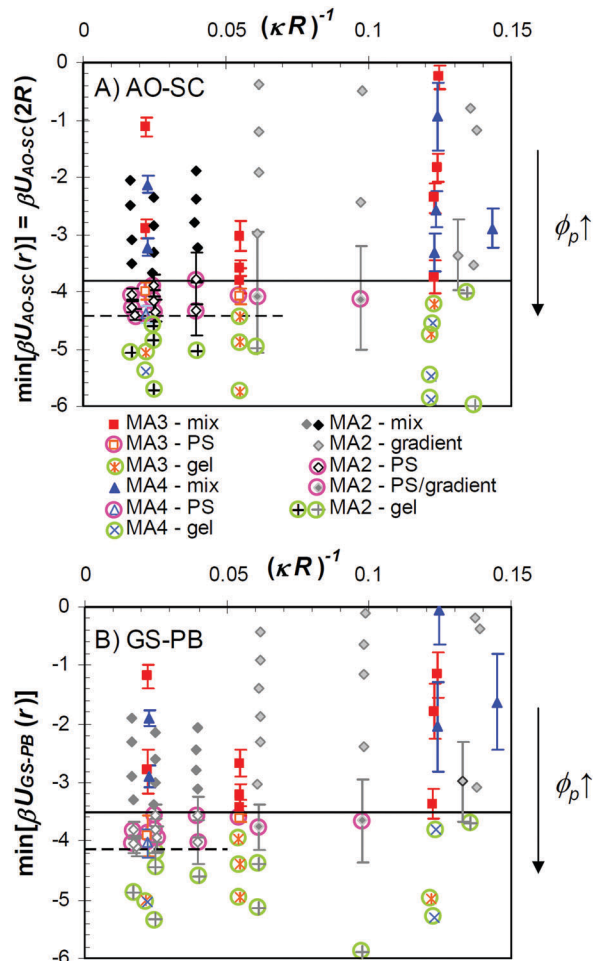


**Fig. 5** State diagram scaled to the minimum in the interaction potential for colloids MA2 (black/grey symbols), MA3 (red/orange symbols) and MA4 (blue symbols) with PEO polymer, including samples with $\phi$ between 0.20–0.22 and $\gamma$ between 0.076 and 0.085, and modelled by (A) AO–SC interactions, or (B) GS–PB interactions. Error bars correspond to those for $Z_{eff}$ in Fig. 4, and are only partly shown to improve readability. Black, red and dark blue symbols refer to modelled results, while grey, orange and light blue symbols are based on estimated or extrapolated values. Continuous lines depict the onset of phase behaviour other than samples being visually homogeneous, while dashed lines indicate the gel transition for high salt/low $(\kappa R)^{-1}$ samples.

perfectly follow the first phase transition at $\min[\beta U_{AO-SC}(r)] = -3.8 \pm 0.1$. To allow a more complete comparison later on for the reduced second virial coefficient, the remaining $Z_{eff}$ values for colloids MA2 are estimated such that the state points follow the trends in Fig. 5, with a single $Z_{eff}$ per salt concentration. The thus established values for $Z_{eff,SC}$ for $c_s \geq 3$ mM and $Z_{eff,PB}$ for all salt concentrations are shown as grey-shades in Fig. 4C and D. Especially the GS–PB results show a remarkable level of charge renormalization under strong screening conditions ($c_s \geq 20$ mM).

For the samples that show a second phase transition from fluid/fluid phase separation to gelation ($c_s \geq 3$ mM), the transition can arguably be drawn at a defined contact potential for $c_s \geq 20$ mM or $(\kappa R)^{-1} < 0.05$. The gel lines would then be at $\min[\beta U_{AO-SC}(r)] = -4.45 \pm 0.1$ and $\min[\beta U_{GS-PB}(r)] = -4.15 \pm 0.1$.

For $c_s \leq 8$ mM or $(\kappa R)^{-1} > 0.05$, the gel transition gradually increases and seems to merge with the lines at $\min[\beta U_{\text{AO–SC}}(r)] = -3.8$ and $\min[\beta U_{\text{GS–PB}}(r)] = -3.5$. It could also be argued that the gel line is described by a continuous slope. Many more data points close to the gel transition should be explored to confirm either way.

### 3.3 Rescaled state diagram with $B_2{}^*$

The contact potential used to rescale the state diagram in Fig. 5 represents a single-point characterization of the overall interactions focussing on the short-range attractive part only. As such, it is not too surprising that the two different model descriptions used here yield slightly different absolute values for the phase transitions. As discussed in the introduction, the reduced second virial coefficient forms an integral measure of the whole interaction potential, and should be model-independent.

Thus, the interaction potential in each state point is integrated into $B_2{}^*$. To increase the readability of the state diagram, the Baxter stickiness parameter $\tau \equiv 1/[4(1 - B_2{}^*)]$ is plotted in Fig. 6 as a function of the range of the repulsions, expressed as $(\kappa R)^{-1}$. Indeed, both the onset of phase separation and the onset of gelation for $(\kappa R)^{-1} < 0.05$ are found to obey the ELCS within the uncertainty of our calculations; with the model-independent spinodal at $\tau = 0.120 \pm 0.005$ and $B_2{}^* = -1.08 \pm 0.08$, and gelation at $\tau = 0.07 \pm 0.01$ and $B_2{}^* = -2.6 \pm 0.5$ for $\phi \approx 0.20$ to $0.22$ and $\gamma = 0.076$ to $0.085$.

Starting from $c_s = 20$ mM ($(\kappa R)^{-1} > 0.04$), the 10% uncertainty in the modelling of $Z_{\text{eff}}$ from scattering data results in a significant uncertainty in $B_2{}^*$ and $\tau$. Strikingly, the manually determined error bars for $Z_{\text{eff}}$ in Fig. 4, displaying strong variation with salt concentration, translate to error bars that are basically salt-independent on an absolute, linear scale for the contact potential in Fig. 5 and on a relative, logarithmic scale for $\tau$ in Fig. 6.

For $(\kappa R)^{-1} > 0.05$, the rescaling starts to break down, with phase transitions moving towards higher $\tau$ values, and with the absolute $\tau$ values at the phase transitions becoming model-dependent. Recently, it was suggested that for short-range attractive colloids interacting *via* electrostatic repulsions that are longer-ranged than the colloid size, the phase diagram can be rescaled with the attractive part of the interaction potential; *i.e.* $U(r)$ for $2R < r < r_0$ for which $U(r_0) = 0$.[47] Applying the $B_2{}^*$-scaling to this part of the potential brought the phase transitions closer to those for $(\kappa R)^{-1} < 0.05$ (data not shown). However, they remained higher in absolute values, as well as model dependent.

In summary, within the here described approach ELCS-rescaling seems to capture the onset of phase separation as well as the onset of gelation for $(\kappa R)^{-1} < 0.05$ at a fixed colloid concentration. This should be taken with caution due to the limited number of samples taken close to the phase transitions, the intrinsic model uncertainty, and the fact that the critical colloid concentration could change with the range of the repulsions. In contrast, the scaling clearly breaks down for longer ranged repulsions. If we take a closer look at the interaction potentials for colloids MA2 (Fig. 7), this transition seems to correspond to the repulsions becoming longer ranged
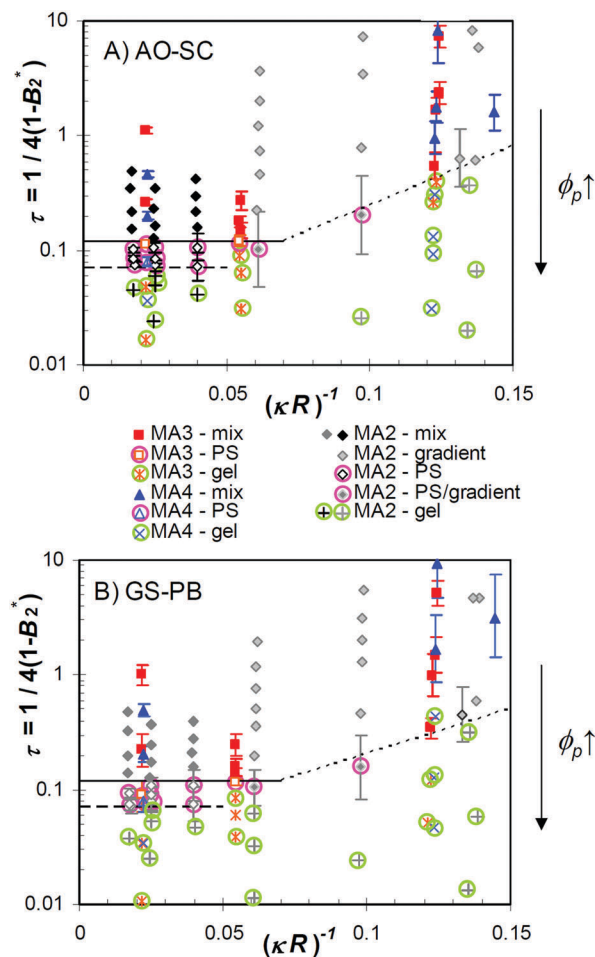


Fig. 6 State diagram scaled to $B_2{}^*$ for colloids MA2 (black/grey symbols), MA3 (red/orange symbols) and MA4 (blue symbols) with PEO polymer, including samples with $\phi$ between $0.20–0.22$ and $\gamma$ between $0.076$ and $0.085$, and modelled by (A) AO–SC interactions, or (B) GS–PB interactions. Error bars correspond to those for $Z_{\text{eff}}$ in Fig. 4, and are only partly shown to improve readability. Black, red and dark blue symbols refer to modelled results, while grey, orange and light blue symbols are based on estimated or extrapolated values. Continuous lines depict the onset of phase behaviour other than samples being visually homogeneous, while dashed lines indicate the gel transition for high salt/low $(\kappa R)^{-1}$ samples. Dotted lines are dawn to guide the eye for the phase boundary of low salt/high $(\kappa R)^{-1}$ samples.

than the attractions. Indeed, for $(\kappa R)^{-1} > 0.05$ the interaction potentials close to the phase transitions consistently show a local DLVO-type maximum in the interaction potential with $\max[\beta U(r)] > 0.1$ for $r \approx 2R\gamma'$.

### 3.4 Nature of the inhomogeneities

Below a certain salt concentration several phenomena occur in the colloid/polymer mixtures, that differ from typical short-range attractive systems: (1) large inhomogeneities appear in the mixtures as characterized by the THPs; (2) the effective surface charge contributing to the repulsive part of the potential shows significant charge renormalization as a function of colloid and polymer concentration; (3) the interaction potential features a local maximum; and (4) phase transitions
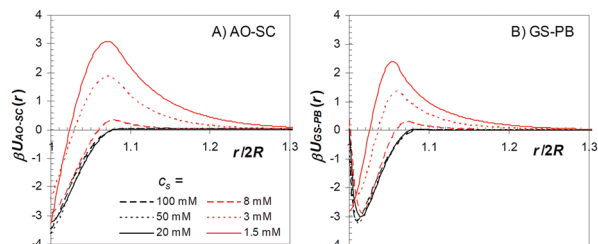
**Fig. 7** Interaction potentials for mixtures of colloids MA2 and PEO at the highest PEO concentration for which the samples are visually homogeneous, calculated using (A) Asakura–Oosawa attractions and screened Coulomb repulsions (AO–SC), and (B) good solvent attractions and mimicked Poisson–Boltzmann repulsions (GS–PB). $Z_{eff}$ values are estimated, as described in the text (Fig. 4C and D).



**Fig. 8** (A) SANS structure factors of mixtures of colloids MA3 and PEO with $c_s$ = 1.5 mM for $\phi$ = 0.22. (B) SESANS data of mixtures of colloids MA3 and PEO with $c_s$ = 1.5 mM for $\phi$ = 0.21.

cannot be rescaled using the ELCS. For colloids MA2, this transition occurs upon a decrease of the salt concentration from 20 to 8 mM (*i.e.* an increase of $(\kappa R)^{-1}$ from 0.04 to 0.06). Since for colloids MA3 no THPs could be measured, it is not certain whether the samples with 8 mM salt (*i.e.* $(\kappa R)^{-1}$ = 0.055) show the same inhomogeneities, or not. However, the interaction potentials of MA3 with 8 mM salt feature a local maximum around $0.2kT$.

Bearing in mind the formation of well-defined clusters for longer-ranged repulsions,[16–21,47] the observed inhomogeneities could be linked to the presence of larger clusters, that dramatically change the forward scattering of the samples compared to well-dispersed repulsive colloids. To create the vertical gradients, these clusters should be prone to gravity, which means that their size, $R_c$, approaches the sedimentation length, $l_{sed} = 3k_BT/(4\pi R_c^3 \Delta \rho g)$, with $\Delta \rho$ the density mismatch between polystyrene and water and $g$ the gravitational acceleration. This implies dense clusters on the order of at least 1 micron, which contain several 10 s of colloids.

Due to the strong correlations between colloids in such clusters, their existence could be verified by the presence of an intra-cluster peak in the SANS signal, and in SESANS they would affect the signal at larger length scales. The SANS data for colloids MA3 with 1.5 mM salt in Fig. 8A show a clear structure factor peak at $q$ = 0.063 nm$^{-1}$ for the gelled samples. However, even for the highest polymer concentration in the non-gelled samples, there is no trace of a peak at this $q$-value. In line with this, the SESANS data for colloids MA4 with 1.5 mM salt in Fig. 8B are completely flat between 300–1500 nm. A SESANS signal is only flat if there is no structuring in the sample at that length scale, confirming the absence of a significant number of large objects. Additionally, we have attempted to measure height-dependent structure factors of our samples with SAXS, where the illuminating beam is considerably smaller than for SANS (data not shown). No significant differences were observed within the measurement accuracy, indicating that any height-dependent differences in structure are very subtle and that the internal structure is that of a dispersed fluid.

Alternatively to defined (equilibrium) clusters, the fluctuations could be caused by long-lived concentration fluctuations.
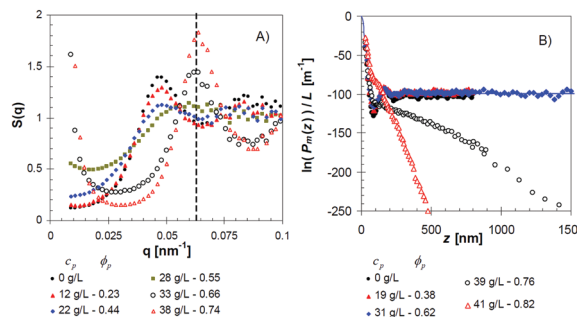
The modelled SANS and SESANS data assume an average interaction potential, that describes the sample as a whole. Imagine the effect of natural concentration fluctuations in a colloid/polymer mixture at low salt concentration, where significant charge renormalization takes place as a function of colloid concentration. In a region concentrated in colloids, the effective surface charge is expected to decrease, reducing the local repulsions. In a colloid-poor region, the effective surface charge could increase, which leads to relatively stronger repulsions. Thus, charge renormalization can enhance concentration fluctuations and ultimately lead to a concentration gradient over the full sample height.

The present data cannot conclusively distinguish between both scenarios. Nevertheless, the difference in time-scale to reach steady state THPs – less than 4 h for $(\kappa R)^{-1}$ < 0.05 and more than 8 h for $(\kappa R)^{-1}$ > 0.05 (Fig. 2B *versus* Fig. 2D and E) – is an indication that the maximum in the interaction potential for $(\kappa R)^{-1}$ > 0.05 and the continuous charging/discharging significantly increase the time for the sample to reach (meta-)equilibrium.

### 3.5 Generic state diagram

To place these results into perspective, the phase transition from a homogeneous fluid to a phase separating state (either or not gelled) is compared to literature data in Table 3 for colloids that are considered to interact *via* attractions only, and zooming-in on a colloid volume fraction of $\phi \approx 0.2$. Despite numerous attempts to define generic phase behaviour for short-range attractive colloids, the available experimental data vary significantly; both quantitatively for the rescaled transition expressed as $\tau$ as well as phenomenologically. A distinction exists between studies that observe a transition from a homogeneous fluid to a (meta-) stable fluid–fluid (FF) and/or fluid-crystal (FC) coexistence,[48,50,51] and those that find a transition from a homogeneous fluid to a space-spanning gel.[3,49,52]

A common explanation of the observed differences, is the effect of gravity.[3] Indeed, the systems showing a defined FF or FC coexistence region tend to have a significant density mismatch between the colloids and the solvent ($\Delta \rho_g$), allowing gravity to interfere with the phase behaviour.[5,48–51,53] Intriguingly, the disappearance of a FF or FC coexistence was previously linked

**Table 3** Comparison with literature data for the single fluid to phase separated and/or gel transition for short-range attractive colloids with supposedly fully screened repulsions

| $\tau^a$ $\phi \approx 0.2$ | $\phi$ studied | $\gamma$ | Colloids[b] | $R$ [nm] | Ref. |
|---|---|---|---|---|---|
| $0.120 \pm 0.005$ | 0.2 | 0.08 | Polystyrene | 60 | This work[c] |
| $0.13 \pm 0.1$ | 0.045 to 0.16 | 0.059 | PMMA | 560 | 3 |
| $0.15 \pm 0.02$ | 0.05 to 0.65 | 0.035–0.05 | MFA | 82 | 48 |
| $0.18 \pm 0.1$ | 0.05 to 0.4 | 0.008 | Silica | 38 | 49 |

| $c/c_p{}^{*a}$ for $\phi \approx 0.2$ | $\phi$ studied | $\gamma$ | Colloids | $R$ [nm] | Ref. |
|---|---|---|---|---|---|
| $0.28 \pm 0.01$ | 0.1 to 0.65 | 0.062 | PMMA | 162 | 50 |
| $0.225 \pm 0.005$ | 0.045 to 0.16 | 0.059 | PMMA | 560 | 3 |
| $0.17 \pm 0.01$ | 0.2 | 0.08 | Polystyrene | 60 | This work[c] |
| $0.14 \pm 0.02$ | 0.02 to 0.65 | 0.08 | PMMA | 220 | 51 |
| $0.090 \pm 0.005$ | 0.03 to 0.4 | 0.060 | Silica | 59 | 52 |

[a] Uncertainty reflects accuracy of reading out the data from graphs. [b] PMMA = poly(methyl methacrylate); MFA = poly(tetra-fluoro-ethylfluoromethyl ether). [c] For $c_s = 100$ mM, $\kappa R \approx 60$.

to the range of repulsions becoming of the order of magnitude of, or surpassing the range of the attractions.[46] The systems showing a transition from homogeneous fluid to a gel tend to consist of PMMA particles in organic solvents, where no reference is being included to whether residual charges are being screened,[21,54,55] or where residual repulsions are considered negligible.[3,56]

We sum up our findings in the generic state diagram in Fig. 9 for the experimental reality of colloids that interact *via* short-range attractions and screened Coulomb repulsions with a variable range. We define the range of the repulsions, $\gamma_{ES}$, as a function of the height of the electrostatic potential, rather than by the Debye length only, with $\beta U_{ES}(2R[\gamma_{ES} + 1]) = 0.1$.

For predominantly attractive systems, the phase behaviour in the presence of repulsions can be fully rescaled following the ELCS. Here, our results are quantitatively in line with comparable systems described in literature, either with[48,50,51] or without[3]



**Fig. 9** Generic state diagram of short-range attractive colloids with variably ranged repulsions, including the experimental reality of residual vdW attractions and density mismatches. The total interactions are captured in the reduced second virial coefficient, $B_2^*$ and the contact potential, $\min[U(r)]$, and the range of the repulsions, $\gamma_{ES}$, is taken as the point where the electrostatic potential has a value of $\beta U_{ES}(2R[\gamma_{ES} + 1]) = 0.1$. Dashed and dash-dotted lines refer to tentative phase boundaries.

gravity playing a role. Small discrepancies may originate from the experimental techniques used to determine the effective colloid volume fraction,[57] and those to model the interactions (microscopy with particle tracking,[3] scattering, sedimentation profiles[48]), as well as the effects of colloidal softness due to steric stabilization,[6] and the source of the attractions. It remains an open question whether a FF/FC window is intrinsic to such systems or only due to gravity. Though the present system can be density-matched in an appropriate mixture of $H_2O$ and $D_2O$, it fell outside the scope of this study to explore this complementary dimension to the phase diagram. Such an extension would be an extremely insightful addition to the available experimental data.

For intermediate-ranged repulsions, both the qualitative phase behaviour and the scaling *via* the ELCS break down once the repulsions become longer-ranged than the attractions. The FF-separation window seems to disappear for $c_s \leq 1.5$ mM, which corresponds to $\gamma_{ES} > 0.15$. This might be linked to many-body interactions starting to play a role for interactions beyond a range of 0.15.[58,59] To distinguish between the different effects on the exact phase diagram, a larger parameter space should be investigated, for instance by varying $\gamma$, $\phi$, and $\Delta\rho_g$.

In the limit of repulsions that are longer-ranged than the particle size, a transition is expected to equilibrium cluster formation and gelation, probably around $\gamma_{ES} \approx 1$. As equilibrium gels are rather different from the spinodal decomposition gels formed for predominantly attractive systems, it is likely that the gels formed at intermediate ranges of the repulsions follow a somewhat different route than either one. Indeed, significantly different gel structures have been observed by microscopy for intermediate ranged repulsions ($\kappa R$ between 7 and 15).[46,60] Though the shape of the potentials are rather close to DLVO-type colloids, the mechanism for gelation will be quite different without the strong vdW trap to induce permanent colloid aggregation.

## 4 Conclusions

In summary, we have established the state diagram of short-range attractive colloids with electrostatic repulsions that are carefully tuned to determine the effect of the repulsions becoming longer-ranged than the attractions. We demonstrate that for predominantly attractive systems, the phase behaviour is pheno-menologically equal to purely short-range attractive systems. The onset of fluid–fluid phase separation and gelation can be rescaled with the reduced second virial coefficient and with the contact potential. Below a well-defined salt concentration, large inhomo-geneities and gradients develop in the samples and the transitions only scale with the contact potential. The repulsions becoming longer ranged than the attractions changes the static and dynamic properties of the colloid–polymer mixtures and causes the FF-coexistence gap to disappear. As mixed potentials of comparable range are likely to be found in real systems, it is important to better understand their impact on phase behaviour.

We summarize our results in a generic state diagram for short-range attractive systems with variably ranged electrostatic repulsions. Due to experimental constraints, the actual phase
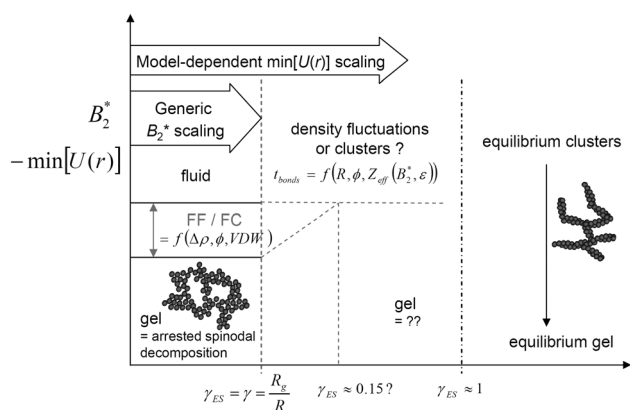
behaviour will always be influenced by the density mismatch between the colloids and the solvent, and by residual vdW attractions. Moreover, we clearly show that residual repulsions have a profound effect on the state diagram, both quantitatively and qualitatively. We believe that basically all experimental model systems to study short-range attractive interactions will have to address residual repulsions. Those repulsions should always be discussed in their full shape, being a combination of Debye length and effective charges, including the degree of charge renormalization.

As a link to the limit of repulsions that are also longer ranged than the colloid size combined with short-range attractions, our results form only a first exploration. In addition to the commonly known interference of residual vdW attractions and gravity with phase behaviour, charge renormalization should be kept in mind as well. Considering that each experimental model system has its own drawbacks, it is paramount that a variety of colloids is used to study the intriguing and relevant phase behaviour for competing attractions and repulsions.

## Conflicts of interest

There are no conflicts of interest to declare.

## Acknowledgements

## References

1 A. Donald, *Nat. Mater.*, 2004, **3**, 579–581.

2 R. Mezzenga, P. Schurtenberger, A. Burbidge and M. Michel, *Nat. Mater.*, 2005, **4**, 729–740.

3 P. J. Lu, E. Zaccarelli, F. Ciulla, A. B. Schofield, F. Sciortino and D. A. Weitz, *Nature*, 2008, **453**, 499–504.

4 E. Zaccarelli, P. J. Lu, F. Ciulla, D. A. Weitz and F. Sciortino, *J. Phys.: Condens. Matter*, 2008, **20**, 494242.

5 T. Gibaud, F. Cardinaux, J. Bergenholtz, A. Stradner and P. Schurtenberger, *Soft Matter*, 2011, **7**, 857–860.

6 C. P. Royall, W. C. K. Poon and E. R. Weeks, *Soft Matter*, 2013, **9**, 17–27.

7 A. Lomakin, N. Asherie and G. B. Benedek, *Proc. Natl. Acad. Sci. U. S. A.*, 1999, **96**, 9465–9468.

8 C. Gögelein, G. Nägele, R. Tuinier, T. Gibaud, A. Stradner and P. Schurtenberger, *J. Chem. Phys.*, 2008, **129**, 085102.

9 M. G. Noro and D. Frenkel, *J. Chem. Phys.*, 2000, **113**, 2941–2944.

10 A. Fortini, M. Dijkstra and R. Tuinier, *J. Phys.: Condens. Matter*, 2005, **17**, 7783–7803.

11 C. Gogelein and R. Tuinier, *Eur. Phys. J. E: Soft Matter Biol. Phys.*, 2008, **27**, 171–184.

12 K. Van Gruijthuijsen, R. Tuinier, J. M. Brader and A. Stradner, *Soft Matter*, 2013, **9**, 9977–9982.

13 W. C. K. Poon, S. U. Egelhaaf, P. A. Beales, A. Salonen and L. Sawyer, *J. Phys.: Condens. Matter*, 2000, **12**, L569–L574.

14 H. Sedgwick, J. E. Cameron, W. C. K. Poon and S. U. Egelhaaf, *J. Chem. Phys.*, 2007, **127**, 125102.

15 W. C. K. Poon, *Phys. Rev. E: Stat. Phys., Plasmas, Fluids, Relat. Interdisc. Top.*, 1997, **55**, 3762–3764.

16 A. D. Dinsmore, P. L. Dubin and G. M. Grason, *J. Phys. Chem. B*, 2011, **115**, 7173–7174.

17 F. Cardinaux, E. Zaccarelli, A. Stradner, S. Bucciarelli, B. Farago, S. U. Egelhaaf, F. Sciortino and P. Schurtenberger, *J. Phys. Chem. B*, 2011, **115**, 7227–7237.

18 A. Stradner, H. Sedgwick, F. Cardinaux, W. C. K. Poon, S. U. Egelhaaf and P. Schurtenberger, *Nature*, 2004, **432**, 492–495.

19 A. I. Campbell, V. J. Anderson, J. S. van Duijneveldt and P. Bartlett, *Phys. Rev. Lett.*, 2005, **94**, 208301.

20 H. Sedgwick, S. U. Egelhaaf and W. C. K. Poon, *J. Phys.: Condens. Matter*, 2004, **16**, S4913–S4922.

21 P. N. Segre, V. Prasad, A. B. Schofield and D. A. Weitz, *Phys. Rev. Lett.*, 2001, **86**, 6042–6045.

22 F. Sciortino, S. V. Buldyrev, C. De Michele, G. Foffi, N. Ghofraniha, E. La Nave, A. Moreno, S. Mossa, I. Saika-Voivod, P. Tartaglia and E. Zaccarelli, *Comput. Phys. Commun.*, 2005, **169**, 166–171.

23 E. Zaccarelli, *J. Phys.: Condens. Matter*, 2007, **19**, 323101.

24 R. Hidalgo-Alvarez, A. Martin, A. Fernandez, D. Bastos, F. Martinez and F. J. De las Nieves, *Adv. Colloid Interface Sci.*, 1996, **67**, 1–118.

25 C. P. Royall, M. E. Leunissen and A. van Blaaderen, *J. Phys.: Condens. Matter*, 2003, **15**, S3581–S3596.

26 K. Van Gruijthuijsen, M. Obiols-Rabasa, M. Heinen, G. Nägele and A. Stradner, *Langmuir*, 2013, **29**, 11199–11207.

27 K. Van Gruijthuijsen, W. G. Bouwman, P. Schurtenberger and A. Stradner, *Europhys. Lett.*, 2014, **106**, 28002.

28 H. N. W. Lekkerkerker and R. Tuinier, *Colloids and the Depletion Interaction*, Springer, Heidelberg, Germany, 2011.

29 K. W. Ebagninin, A. Benchabane and K. Bekkour, *J. Colloid Interface Sci.*, 2009, **336**, 360–367.

30 S. Kawaguchi, G. Imai, J. Suzuki, A. Miyahara and T. Kitano, *Polymer*, 1997, **38**, 2885–2891.

31 S. Kinugasa, H. Nakahara, N. Fudagawa and Y. Koga, *Macromolecules*, 1994, **27**, 6889–6892.

32 K. Devanand and J. C. Selser, *Macromolecules*, 1991, **24**, 5943–5947.

33 B. Vincent, P. F. Luckham and F. A. Waite, *J. Colloid Interface Sci.*, 1980, **73**, 508–521.

34  D. Vivares, L. Belloni, A. Tardieu and F. Bonnete, *Eur. Phys. J. E: Soft Matter Biol. Phys.*, 2002, **9**, 15–25.

35  J. Kohlbrecher and W. Wagner, *J. Appl. Crystallogr.*, 2000, **33**, 804–806.

36  U. Keiderling, *"BerSANS" Data Reduction Program*, version: 26-Jun-2008, HMI Berlin, Berlin, 1994–2008.

37  M. T. Rekveldt, J. Plomp, W. G. Bouwman, W. H. Kraan, S. Grigoriev and M. Blaauw, *Rev. Sci. Instrum.*, 2005, **76**, 033901.

38  R. Andersson, L. F. van Heijkamp, I. M. de Schepper and W. G. Bouwman, *J. Appl. Crystallogr.*, 2008, **41**, 868–885.

39  F. Xie, M. Turesson, C. E. Woodward, K. Van Gruijthuijsen, A. Stradner and J. Forsman, *Phys. Chem. Chem. Phys.*, 2016, **18**, 11422–11434.

40  G. J. Fleer and R. Tuinier, *Adv. Colloid Interface Sci.*, 2008, **143**, 1–47.

41  J. K. Percus and G. J. Yevick, *Phys. Rev.*, 1958, **110**, 1–13.

42  D. Gazzillo and A. Giacometti, *J. Chem. Phys.*, 2000, **113**, 9837–9847.

43  *Neutrons, X-rays and Light: Scattering Methods Applied to Soft Condensed Matter*, ed. P. Lindner and T. Zemb, Elsevier Science B. V., Amsterdam, The Netherlands, 2002.

44  J. Kohlbrecher and A. Studer, *J. Appl. Crystallogr.*, 2017, **50**, 1395–1403.

45  A. P. Gast, W. B. Russel and C. K. Hall, *J. Colloid Interface Sci.*, 1986, **109**, 161–171.

46  C. P. Royall, D. Aarts and H. Tanaka, *J. Phys.: Condens. Matter*, 2005, **17**, S3401–S3408.

47  P. Douglas Godfrin, N. E. Valadez-Perez, R. Castaneda-Priego, N. J. Wagner and Y. Liu, *Soft Matter*, 2014, **10**, 5061–5071.

48  S. Buzzaccaro, R. Rusconi and R. Piazza, *Phys. Rev. Lett.*, 2007, **99**, 098301.

49  H. Verduin and J. K. G. Dhont, *J. Colloid Interface Sci.*, 1995, **172**, 425–437.

50  S. M. Liddle, T. Narayanan and W. C. K. Poon, *J. Phys.: Condens. Matter*, 2011, **23**, 194116.

51  W. C. K. Poon, J. S. Selfe, M. B. Robertson, S. M. Ilett, A. D. Pirie and P. N. Pusey, *J. Phys. II*, 1993, **3**, 1075–1086.

52  S. A. Shah, S. Ramakrishnan, Y. L. Chen, K. S. Schweizer and C. F. Zukoski, *Langmuir*, 2003, **19**, 5128–5136.

53  J. M. Kim, J. Fang, A. P. R. Eberle, R. Castaneda-Priego and N. J. Wagner, *Phys. Rev. Lett.*, 2013, **110**, 208302.

54  M. Laurati, G. Petekidis, N. Koumakis, F. Cardinaux, A. B. Schofield, J. M. Brader, M. Fuchs and S. U. Egelhaaf, *J. Chem. Phys.*, 2009, **130**, 134907.

55  T. Ohtsuka, C. P. Royall and H. Tanaka, *Europhys. Lett.*, 2008, **84**, 46002.

56  P. J. Lu, J. C. Conrad, H. M. Wyss, A. B. Schofield and D. A. Weitz, *Phys. Rev. Lett.*, 2006, **96**, 028306.

57  W. C. K. Poon, E. R. Weeks and C. P. Royall, *Soft Matter*, 2012, **8**, 21–30.

58  G. J. Fleer and R. Tuinier, *Phys. Rev. E: Stat., Nonlinear, Soft Matter Phys.*, 2007, **76**, 041802.

59  S. M. Ilett, A. Orrock, W. C. K. Poon and P. N. Pusey, *Phys. Rev. E: Stat. Phys., Plasmas, Fluids, Relat. Interdisc. Top.*, 1995, **51**, 1344–1352.

60  R. F. Capellmann, N. E. Valadez-Perez, B. Simon, S. U. Egelhaaf, M. Laurati and R. Castaneda-Priego, *Soft Matter*, 2016, **12**, 9303–9313.